

## Relating Lightning Features and Topography over the Tibetan Plateau Using the World Wide Lightning Location Network Data

Hiroyuki IWASAKI

*Faculty of Education, Gunma University, Maebashi, Japan*

*(Manuscript received 12 August 2015, in final form 5 July 2016)*

### Abstract

Lightning features over the Tibetan Plateau were studied in relation to topography using the World Wide Lightning Location Network (WWLLN) dataset obtained from April 2009 until December 2014. To describe the strength of lightning strokes, lightning strokes with energies above the 90th percentile (7666 J) were defined as strong lightning (S-lightning) strokes, and the ratio of S-lightning strokes to the overall number of lightning (O-lightning) strokes was defined as the strong ratio (S-ratio).

O-lightning density over the Tibetan Plateau was found to be high in general, except over the western part of analysis region. Minimum-density zones were observed along the Himalayas approximately 6 km above sea level and in deep valleys within the Tibetan Plateau. The maximum- and minimum-density zones also exhibited maximum and minimum annual rainfall amounts, respectively. S-lightning strokes were also found to frequently occur over the Tibetan Plateau, and most S-ratios in the analysis units exceeded 30 %, which corresponds to three times the global mean. In particular, the S-ratios over the southern part of the Tibetan Plateau, including the Himalayas, were found to be high (50 %) and to correspond with the zone that had the minimum O-lightning density.

The maximum O-lightning density was observed to occur during the summer at an elevation approximately 0.2–1.0 km higher than the plateau level. The O-lightning and S-lightning densities around the Nagqu sonde station were negatively correlated with the Showalter stability index (SSI) and the vertical wind shear. The S-ratio and average stroke energy were found to be negatively correlated with the vertical shear but not with the SSI.

**Keywords** lightning; Tibetan Plateau; WWLLN; topography

### 1. Introduction

The features of the deep convection above the Tibetan Plateau have been studied to better understand their impacts on large-scale climate events (e.g., Yanai and Li 1994) and to improve our understanding of the meteorology of very high mountainous regions (e.g., Yamada and Uyeda 2006). It is well known that numerous thunderstorms develop above the Tibetan Plateau; however, only a few investigations pertaining

to lightning exist due to a lack of local observational data. Lightning features over the Tibetan Plateau were fragmentarily described in globally conducted studies of lightning climatology using lightning flash data derived from the satellite-borne optical sensors of the Defense Meteorological Satellite Program (e.g., Orville and Henderson 1986), Optical Transient Detector (OTD) (e.g., Christian et al. 2003), and Tropical Rainfall Measuring Mission Lightning Imaging Sensor (TRMM/LIS) (Qie et al. 2003; Houze et al. 2007). Using the gridded OTD dataset, Toumi and Qie (2004) found that there is more lightning on the Tibetan Plateau during the spring than would be expected from a simple relation with the rainfall amount and temperature. However, the orbital paths

---

Corresponding author: Hiroyuki Iwasaki, 4-2 Aramaki, Maebashi, Gunma 371-8510, Japan  
E-mail: iwasaki@gunma-u.ac.jp  
J-stage Advance Published Date: 20 July 2016  
©2016, Meteorological Society of Japan

of the abovementioned satellites prevent them from continuously observing specific areas of interest to deepen the understanding of lightning climatology. Therefore, data with greater spatiotemporal coverage are required.

A global lightning dataset, derived from the ground-based World Wide Lightning Location Network (WWLLN), became available in April 2004, and some researchers have addressed features of global and/or regional lightning climatology (Virts et al. 2013; Iwasaki, 2014). Furthermore, compared to data from satellite-borne optical sensors, WWLLN data have the advantage of providing stroke energy information. Iwasaki (2015) indicated that the ratio of strong lightning (i.e., lightning with a stroke energy > 90th percentile for global lightning) to overall lightning over the oceans of the subpolar zones of the Northern and Southern Hemispheres tends to be large (more than 40 %) during the cold season and that the strong ratio (i.e., the ratio of strong lightning strokes to the overall number of strokes) over the Tibetan Plateau is large during the warm season. This large strong ratio over the Tibetan Plateau is a unique feature, which is not exhibited in other very high mountainous regions such as the Rockies and Andes. The aim of this study was to determine the general features of lightning over the Tibetan Plateau according to stroke energy strength using WWLLN data.

## 2. Data

### 2.1 WWLLN data

#### a. Determination of lightning location and energy

Lightning features over the Tibetan Plateau (Fig. 1) were studied using the WWLLN dataset obtained from April 2009 until December 2014. The WWLLN comprises over 70 receiving sites, which monitor the very-low-frequency (VLF) radio waves (6–18 kHz) emitted by lightning strokes. The dispersed waveforms (the so-called “sferics”) of the lightning impulses are processed at each receiving site. The locations of lightning strokes are determined based on the group arrival times of the VLF waves detected at five or more stations and are particularly sensitive to the return cloud-to-ground lightning strokes (Dowden et al. 2002). The WWLLN algorithm can detect lightning strokes with spatial and temporal accuracies of 5 km and 15  $\mu$ s, respectively, and its detection efficiency is 11 % for all strokes and > 30 % for more powerful strokes (Rodger et al. 2004; Abarca et al. 2010). The elevation of each lightning point was determined using a global digital elevation model

(SRTM30\_PLUS Ver11; Becker et al. 2009) with a spatial resolution of 30 arc-s (approximately 1 km).

Using another WWLLN algorithm, radiated VLF stroke energy, which is directly related to the peak current of the return strokes, was re-calculated using the root-mean-square energy from 7–18 kHz with 1.33-ms sample times for all lightning strokes recorded since April 2009 (Hutchins et al. 2012a). The attenuation of each sferic along the great circle path (GCP) was calculated based on an ionospheric model with regard to the influence of its diurnal variation. In comparison with ground-based lightning data detected by IMPACT-ESP2 sensors in New Zealand, the coefficient of determination ( $R^2$ ) for the estimated peak currents between the two sensors was 0.92. Since the stroke energy is less reliable when estimated based on the energy data from fewer than three stations, these data were removed from the dataset (Iwasaki 2015).

#### b. Relative detection efficiency of lightning

The attenuation of the sferics emitted by a lightning stroke is influenced by the surface conductivity and ionospheric electron density along the GCP of the radio wave. There is a larger ionospheric electron density during the daytime in the summer; as a result, the sferic attenuation rate increases and the WWLLN detection efficiency of lightning decreases. A similar change in sferic attenuation over the GCP occurs due to the low conductivities of surfaces covered by snow and/or ice. Furthermore, the minimum detectable energy of lightning is influenced by the density of WWLLN sites. Therefore, the detection efficiency of the WWLLN system is not uniform. To overcome this challenge, Hutchins et al. (2012b) proposed the “relative detection efficiency” (RDE) parameter, which is calculated using the observed 7-day global stroke energy distribution and the estimated hourly minimum detectable energy for every  $5^\circ \times 5^\circ$  grid cell, considering both sferic propagation and the WWLLN site distribution. RDE is defined as the ratio of the number of strokes with energies larger than the minimum detectable energy (MDE) to the overall number of lightning strokes in the 7-day global stroke energy distribution. The influence of variations in the RDE is discussed in Section 3-2.

### 2.2 Sonde data

To investigate the influence of atmospheric conditions on lightning activity, sonde observation data in the mandatory level at Nagqu (“N” in Fig. 1) were used. The launch times of the sonde were 00 UTC and 12 UTC (06 local standard time (LST) and 18 LST).

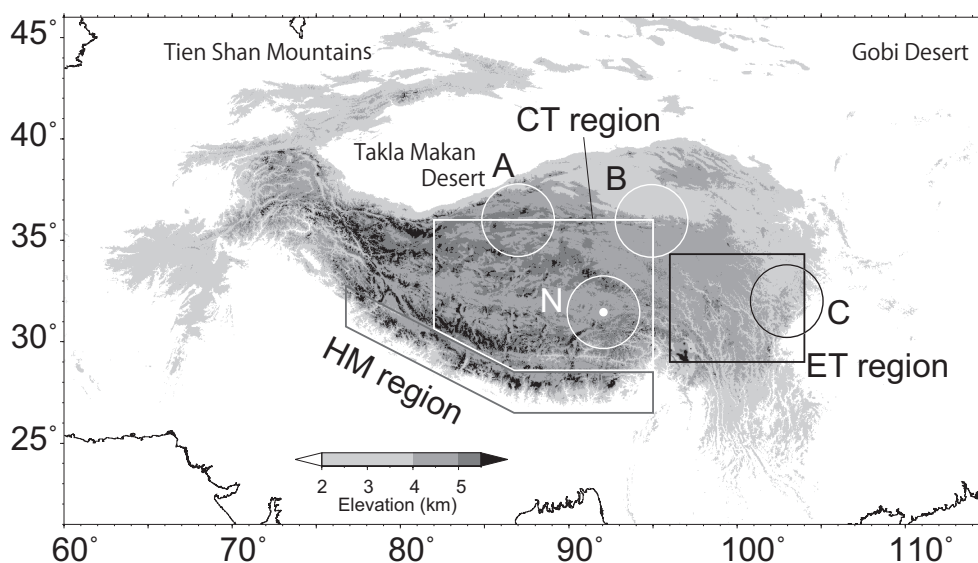


Fig. 1. Map of the analysis region. Polygons indicate three sub-regions: CT, ET, and HM regions. The white dot and circle indicate the location of Nagqu sonde station (N) and 200-km-radius circle around N, respectively. Circles A–C indicate the three analysis units in Fig. 11.

The Showalter stability index (SSI) was adopted as a stability index; however, since the elevation of Nagqu is 4508 m, the ordinary SSI calculation was modified as follows:

$$\text{SSI} = T_{300} - T_{\text{parcel}}, \quad (1)$$

where  $T_{300}$  is the ambient temperature at 300 hPa and  $T_{\text{parcel}}$  is the temperature of a parcel lifted from the surface to 300 hPa, dry-adiabatically to saturation and moist-adiabatically above that.

Additionally, the influence of vertical wind shear, obtained using wind data from 500 hPa and 250 hPa, in an interval roughly corresponding to the section of the atmosphere from above the planetary boundary layer to the upper troposphere, on lightning activity was analyzed.

### 2.3 GSMap products

Hourly Global Satellite Mapping of Precipitation (GSMap) products, which have latitudinal and longitudinal grid resolutions of  $0.1^\circ$ , are used to describe the distributions and temporal variations of rainfall (e.g., Kubota et al. 2007; Ushio et al. 2009). GSMap products used in this study were composed of two data sets: the GSMap\_Microwave-IR Combined product (Ver. 5.22) contains data obtained from April 2009 until November 2010 and the GSMap\_Near\_Real\_Time (GSMap\_NRT) product covers the

period beginning in December 2010. Although the GSMap\_NRT products were calculated using simple algorithms, the two types of GSMap products were analyzed in a same manner in this study. However, the large variation of the emissivities of microwaves over land means that high-precision measurements cannot be expected from GSMap rainfall estimates. Shrestha et al. (2011) showed that the accuracy of GSMap rainfall estimates deteriorates for medium-high and high mountainous regions of the central Himalayas in comparison with flatter terrains. Because of the rain/no-rain classification problems for snow-covered areas, the GSMap microwave radiometer algorithm regards all areas with surface temperatures lower than  $0^\circ\text{C}$  as precipitation-free (Aonashi et al. 2009; Kubota et al. 2007), resulting in the poor performance of the GSMap data there. Therefore, GSMap rainfall data for the cold season (from October until May) above 4 km above sea level (ASL) were not used, and a quantitative analysis of rainfall features was not conducted in this study.

## 3. Analytical methods

### 3.1 S-ratio definition

Figure 2 displays the normalized frequency distribution of stroke energy for all of the lightning in the analysis region and around the world. The normalized frequency was calculated so that the total number of

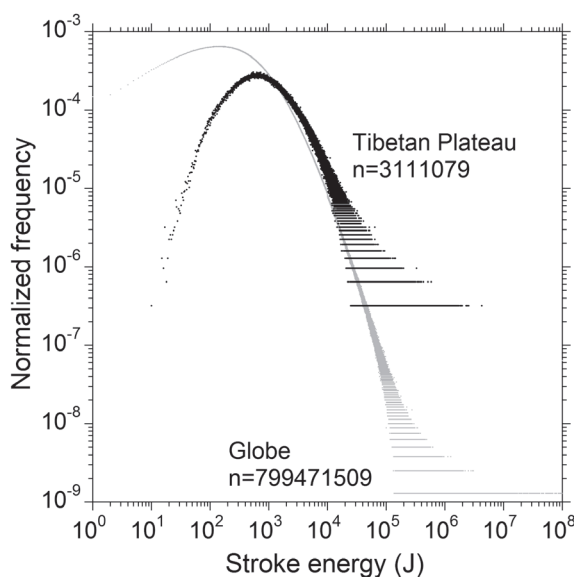


Fig. 2. Normalized frequency distribution of stroke energy for all lightning for the analysis region (black) and world (gray).

lightning strokes in each region would be one. The energy distribution is log-normal, and the dynamic range for stroke energy is very wide, i.e., about 60–70 dB. The mode value of  $6 \times 10^2$  J for the Tibetan Plateau is about three times larger than the global average, which is consistent with the result from Iwasaki (2015) that the ratio of strong lightning over the Tibetan Plateau is more than 1.5 times larger than the global mean.

According to Iwasaki (2015), to describe lightning features based on individual stroke energies, lightning strokes with energies above the 90th percentile (7666 J) globally are defined as strong lightning (S-lightning) strokes, and the ratio of the number of S-lightning strokes to the number of overall lightning (O-lightning) strokes is defined as the strong ratio (S-ratio).

### 3.2 Influence of variations in RDE on S-ratio

Figure 3a shows a season–local time plot of the mean RDE for the study area. The RDE exhibits clear seasonal and diurnal variations corresponding to ionospheric electron density variations. Since the RDE is low in the early afternoon from May until August, while lightning activity is high, as shown in Figs. 5–7 below, lightning strikes with weak stroke energies are difficult to detect, and the S-ratio will be overesti-

mated.

In order to assess the influence of variations in the RDE, we adopted a different S-ratio based on a uniform criterion for the MDE of lightning, so that the quality of the S-ratio would remain uniform regardless of the season and local time. According to the method of Iwasaki (2015), assuming that the stroke energy frequency distributions for all of the grids were similar in shape, all of the lightning strikes with stroke energies above the MDE were detected across the entire grid where the RDE was greater than 0.65. This RDE range covers 93.1 % of all lightning, with an MDE value corresponding to 800 J for the study region. Accordingly, lightning strokes with energies of less than 800 J were not used to calculate the S-ratio reported in this sub-section. The stroke energy of the 90th percentile, which is the criterion for S-lightning considering the MDE, was redefined as 17826 J.

The daily S-ratios, namely, the original S-ratios and the S-ratios considering the MDE, were calculated for the study region, and the relation between them is shown in Fig. 3b. The two S-ratios are well correlated although there are considerable variations. However, the variations are within an acceptable range ( $\pm 5$  %). In addition, we focus on the spatial variations of lightning rather than on temporal variations, so the estimation error due to the RDE variations is not significant. Therefore, the original S-ratios were used without any corrections.

## 4. Results and discussion

### 4.1 Definition of sub-regions

The analysis region was divided into three sub-regions based on topography, GSMaP rainfall amount, and WLLN lightning density. Figure 4 illustrates the distribution of the annual rainfall amount and some lightning features. The lightning density and S-ratio are calculated for every grid with latitudinal and longitudinal resolutions of  $0.1^\circ$ . Rainfall is concentrated along the southern foothills of the Himalayas (Fig. 4a), with lightning density also exhibiting high values in this region (Figs. 4b, c). This area, including the Himalayas, is referred to as the HM region, as shown in Fig. 1. The Tibetan Plateau east of  $80^\circ\text{E}$  shows high densities of O-lightning ( $> 10^{-1}$  stroke  $\text{km}^{-2} \text{yr}^{-1}$ ) and S-lightning ( $> 10^{-1.5}$  stroke  $\text{km}^{-2} \text{yr}^{-1}$ ). In comparison with the central part ( $80$ – $95^\circ\text{E}$ ), the eastern part ( $95$ – $105^\circ\text{E}$ ) is characterized by large rainfall amounts and a lower elevation. These two areas are referred to as the CT region and the ET region, respectively (Fig. 1).

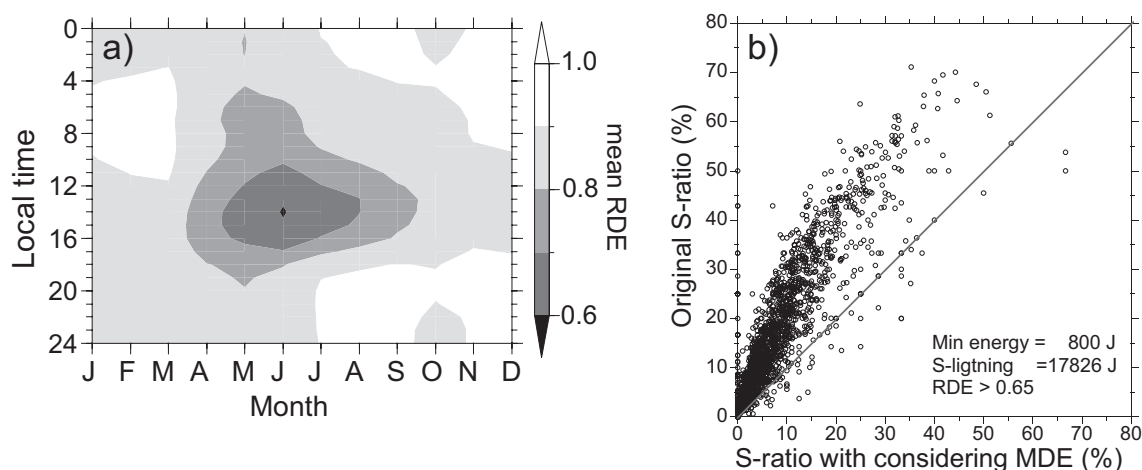


Fig. 3. (a) Season–local time plot of regional mean RDE over Tibetan Plateau. (b) Relation between original S-ratio and S-ratio considering MDE.

#### 4.2 Regional variation of lightning across analysis region

Lightning density across the analysis region varies according to the regional topography. Both the O-lightning and S-lightning densities over the Tibetan Plateau are generally high except in the western part. In addition, the maximum lightning density occurs to the west (windward) of the Himalayas and the Tien Shan Mountains. This maximum density band west of the Himalayas has already been noted based on data from the satellite-borne OTD and TRMM/LIS (Christian et al. 2003; Houze et al. 2007) and corresponds to an area in which deep intense convective echoes were frequently observed by TRMM/PR in June/July/August/September (JJAS) (e.g., Houze et al. 2007). An area with a very low O-lightning density, less than  $10^{-2.5}$  stroke  $\text{km}^{-2} \text{yr}^{-1}$ , runs from the northern part of the Tibetan Plateau to the Takla Makan Desert and the Gobi Desert; a small line of maximum O-lightning density runs along the northern rim of the Tibetan Plateau. In addition, a minimum zone of O-lightning density ( $< 10^{-1.5}$  stroke  $\text{km}^{-2} \text{yr}^{-1}$ ) runs along the Himalayas more than 6 km ASL and in valleys of the Tibetan Plateau. These maximum and minimum areas generally correspond to the maximum and minimum values of GSMaP rainfall, respectively.

Figure 4c shows the distribution of the S-lightning density, which is similar to that of the O-lightning. The S-lightning density over the Tibetan Plateau is relatively high and comparable to that in the southern foothills of the Himalayas. As shown in Fig. 4d, most of the S-ratios in the analysis units exceed 30

% across most of the Tibetan Plateau, which corresponds to three times the global average of 10 %. In particular, the southern part of the Tibetan Plateau, including the Himalayas, shows a very high S-ratio of 50 %. It is noted that the minimum O-lightning density zone along the Himalayas shows a large S-ratio of 50 %. In contrast, a maximum O-lightning density zone over the southern foothills of the Himalayas shows a relatively small S-ratio of less than 20 %. These relations indicate that the regional-scale topography directly influences the density and strength of lightning.

#### 4.3 Diurnal and seasonal lightning variations

##### a. Variations over CT and ET regions

Figures 5 and 6 show the diurnal and seasonal variations in the frequency of GSMaP rainfall above  $0 \text{ mm h}^{-1}$  and some lightning features related to the elevation over the CT and ET regions, respectively. The GSMaP rain and O-lightning density are normalized so that sum of the values in each panel is 100 %. The GSMaP rainfall data more than 4 km ASL were masked for the cold season due to low accuracy; however, the features of the diurnal cycle of GSMaP rainfall for the warm season shown in Figs. 5–7 are consistent with the results from TRMM/PR (Hirose and Nakamura 2005), even for high mountainous regions between 5 km ASL and 8 km ASL.

As shown in Figs. 5a and 6a, nocturnal rainfall (20–05 LST) in June/July/August (JJA) occurs in areas less than 3 km ASL in both regions; however, as the elevation increases, nocturnal rainfall weakens



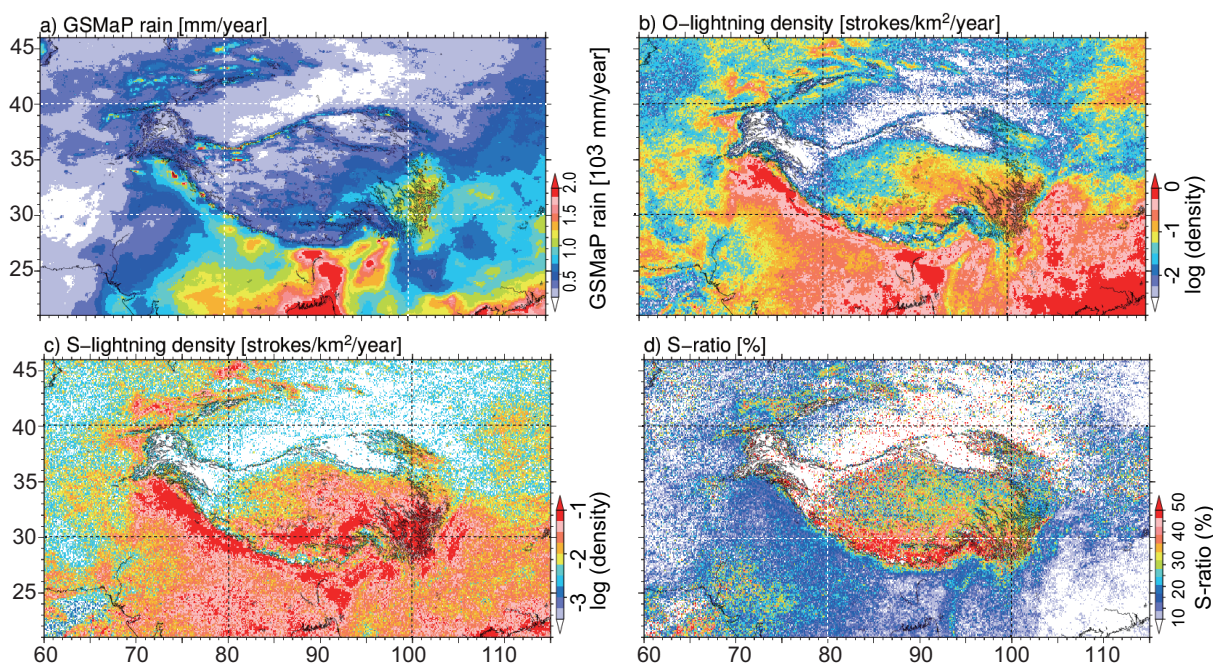


Fig. 4. Distribution of GSMaP rainfall amounts and lightning features across analysis region: (a) GSMaP rainfall amount, (b) O-lightning density, (c) S-lightning density, and (d) S-ratio. Counter indicates an elevation of 4 km ASL.

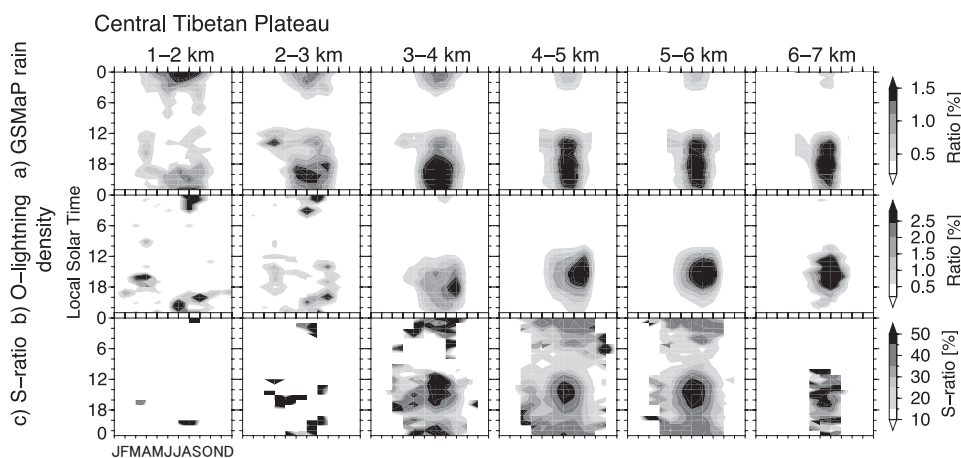


Fig. 5. Season-local time plots of normalized GSMaP rainfall frequency (a: upper panels), normalized O-lightning density (b: middle panels), and S-ratios (c: bottom panels), according to the elevation over CT region. GSMaP rainfall and O-lightning density are normalized so that sum of values in each panel is 100 %. GSMaP rainfall data from October until May for elevations more than 4 km ASL were masked.

and afternoon rainfall (13–24 LST) dominates. Meanwhile, nocturnal O-lightning in the area less than 3 km ASL does not decrease together with rainfall. O-lightning is concentrated in the afternoon (15–18

LST) in the area more than 3 km ASL (Figs. 5b, 6b). It is noted that O-lightning density in September more than 3 km ASL is larger in spite of small GSMaP rainfall amounts in both regions.

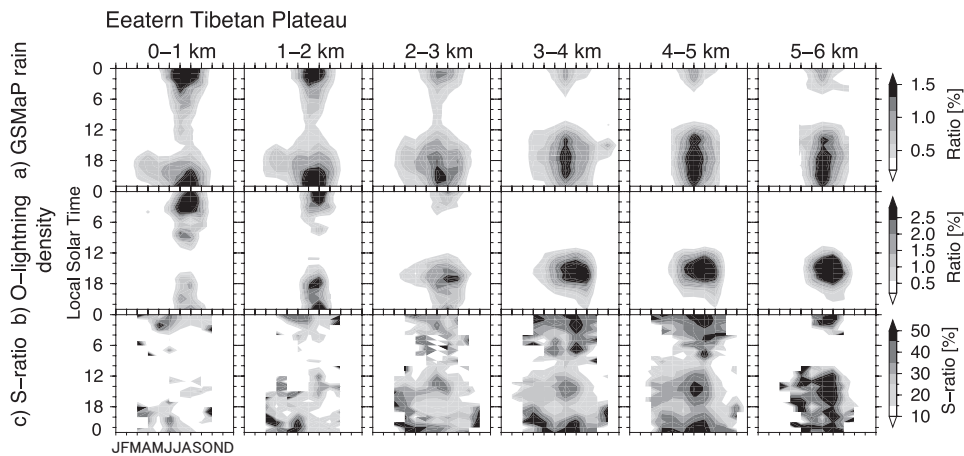


Fig. 6. Same as Fig. 5, but for ET region.

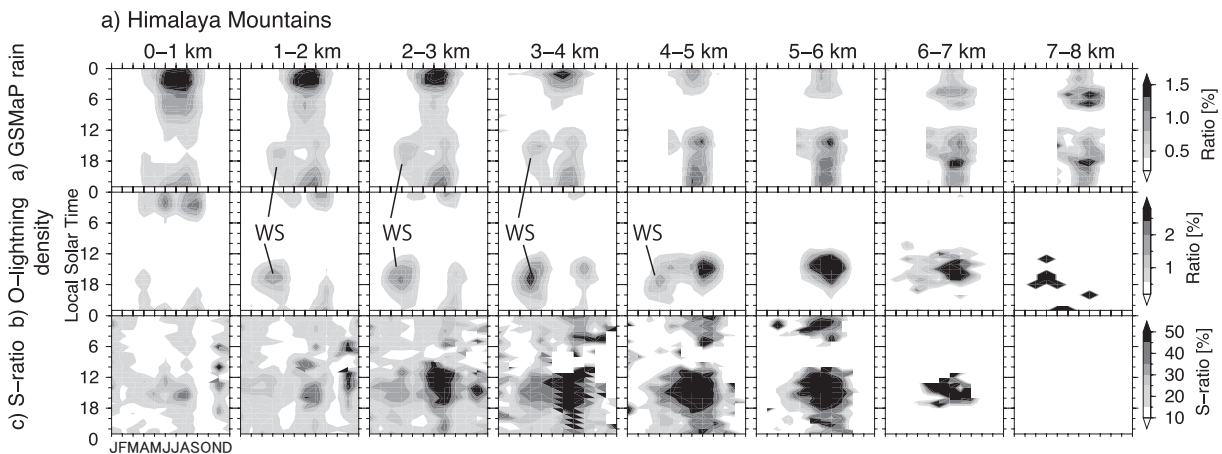


Fig. 7. Same as Fig. 5, but for HM region.

As shown in Figs. 5c and 6c, the S-ratio has two maxima in JJAS: an afternoon maximum (15–18 LST) and a nocturnal maximum (22–02 LST). A large amount of lightning occurs in the evening, whereas at nighttime, the amount of O-lightning is small but the S-ratio is relatively large. These features are common to both regions.

#### b. Variations over HM region

The rainfall frequency over the HM region less than 4 km ASL exhibits a clear midnight maximum, compared with an afternoon maximum more than 4 km ASL in JJA (Fig. 7a). As shown in Fig. 7, most of the O-lightning density peaks (Fig. 7b) correspond to peaks in rainfall frequency (Fig. 7a). However,

in comparison with rainfall frequency's midnight maximum, the O-lightning maxima are very weak at all elevations. The S-ratio has a prominent afternoon maximum (15–18 LST) of more than 45 % and a weak nocturnal maximum (22–02 LST). These features are qualitatively similar to those of the CT and ET regions.

It is interesting that a small maximum can be seen in the afternoon (15–18 LST) in the spring ("WS" in Fig. 7), which corresponds to both the rainfall and lightning maximum zones in the southern foothills of the Himalayas (Figs. 4a–c).

#### 4.4 *Lightning features according to elevation for all three regions*

The previous sub-section pointed out that both the lightning density and S-ratios vary with elevation, and these trends are confirmed by the seasonal variations. Figures 8–10 show monthly elevation profiles of lightning parameters for the warm season. Each lightning parameter is determined for every 100 m in elevation. The right end panels indicate the area profiles for the different elevation zones. A peak is observable for each region, which corresponds to the regional-scale plateau level. Since the CT region has a prominent plateau at 4.9 km ASL and the elevation dependency of the lightning features is relatively clear, the lightning features are mainly described for the CT region in this sub-section.

Figure 8a shows the monthly profiles for the lightning density in 100-m-interval elevation zones over the CT region. The lightning density increases during the monsoon season (JJAS). The maximum lightning density is observable in August, while the lightning density in September is comparable to that in July.

We also considered the profiles above the plateau level of 4.9 km in the CT region (Fig. 8d). The lightning density increases with elevation from the plateau level and reaches a maximum around 5.5 km ASL except in September. Additionally, the S-ratio and average stroke energy also reach maxima above the plateau level; however, those maxima occur 0.2–0.3 km higher than that for the lightning density. It is noted that the lightning activities during the monsoon months (JJAS) are similar for all of the elevation zones in the CT region.

The ET and HM regions in the summer have two features in common with the CT region. First, their maximum lightning densities are observable in August and their lightning densities in September are comparable to those in July. Second, lightning density maxima exist above the plateau level. The elevation profiles of the S-ratio and the average stroke energy in the ET region are similar to those of the lightning density.

#### 4.5 *Lightning features related to local topography*

The previous sub-section pointed out that lightning density variations are influenced by elevation. In this sub-section, to discuss the factors determining the level of the maximum lightning density, we present results obtained by focusing on local topography to increase the sample numbers and the dynamic range at the height of the plateau level. The analysis method is the same as that described in the previous sub-section,

but the analysis units were reduced to 200-km-radius circles, such as circles A–C in Fig. 1. The centers of 18 analysis units were allocated every 4° in longitude from 83°E to 103°E and in latitude from 28°N to 36°N. Since the plateau levels or maximum levels of four of these units were uncertain, they were excluded from the analysis.

Figure 11 shows the O-lightning density elevation profiles and the areas of the elevation zones for three typical units (A–C in Fig. 1). The local features exhibit patterns similar to the regional features, as shown in Figs. 8–10. It is noted that the maximum O-lightning density level seems to be high when the plateau level is higher. To confirm this trend, we compared the plateau levels and the maximum O-lightning density levels in 14 analysis units. As shown in Fig. 12, most of the maximum O-lightning density levels are located about 0.2–1.0 km higher than the plateau levels, and the maximum O-lightning density levels in July and August are correlated with the plateau levels at 5 % significance, while the correlation in September is not significant. It is reasonable to assume that the differential height from the local plateau level is relevant in determining the maximum O-lightning density level. It is well known that moisture transport from the plain to the mountains, and the surface wind convergence at the feet of mountains due to thermally induced local circulation, increase convective activity (e.g., Iwasaki and Miki 2002; Sato and Kimura 2005). Some studies based on TRMM/PR data have indicated that diurnal convective activity variations are controlled by the topography over the Tibetan Plateau (e.g., Bhatt and Nakamura 2005; Singh and Nakamura 2009). Local circulation is a possible factor determining the maximum lightning density level.

#### 4.6 *Influence of atmospheric conditions on lightning features*

Lightning activity is expected to be influenced by atmospheric conditions as well as topography. In this sub-section, we focus on the SSI and vertical wind shear, which significantly influence convective activity. The analysis objects were lightning strikes observed within a 200-km-radius circle around Nagqu at 16–20 LST in JJAS. The SSI and vertical wind shear were calculated using Nagqu sonde data at 18 LST, and days with no lightning were removed from the analysis.

Figure 13 (Fig. 14) shows the relation between the SSI (vertical wind shear) and the lightning parameters. The amounts of both O-lightning and S-lightning



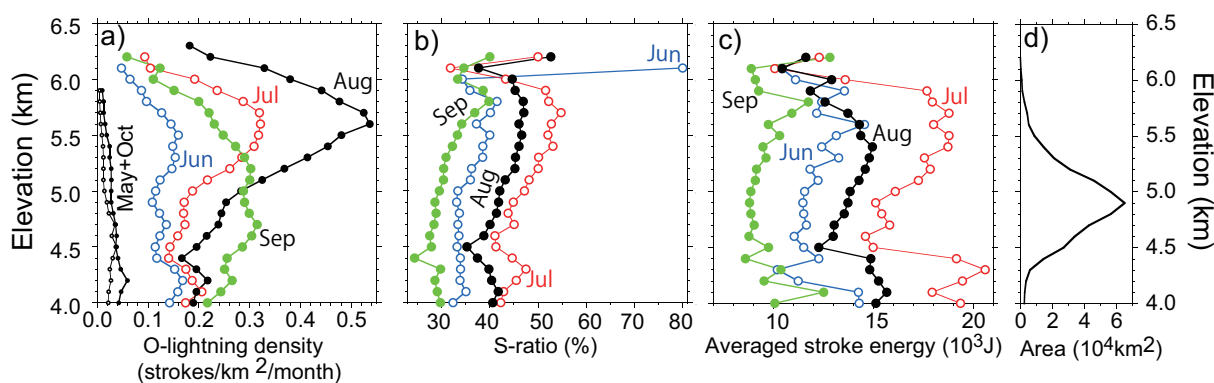


Fig. 8. Monthly elevation profiles of lightning properties calculated for every 100 m of elevation for CT region: (a) O-lightning density, (b) S-ratio, (c) average stroke energy, and (d) area of each elevation zone. Data for elevation zones with fewer than 10 observations are not plotted.

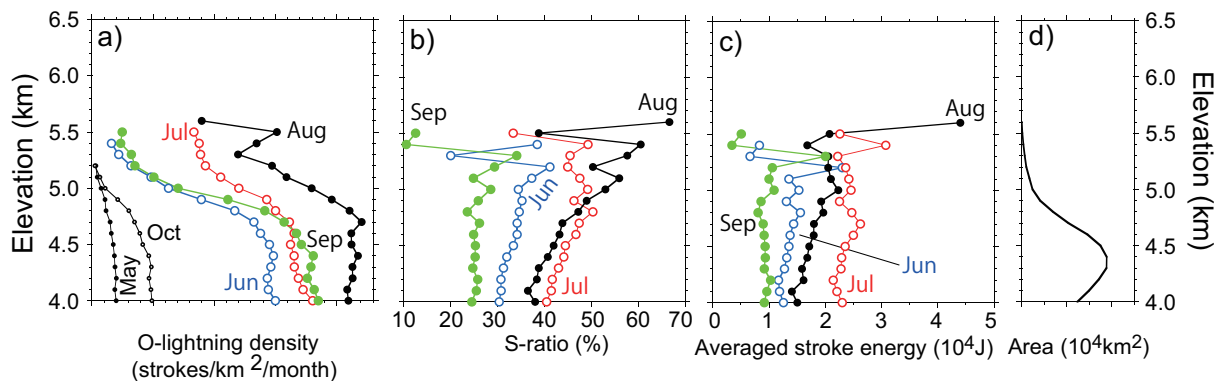


Fig. 9. Same as Fig. 8, but for ET region.

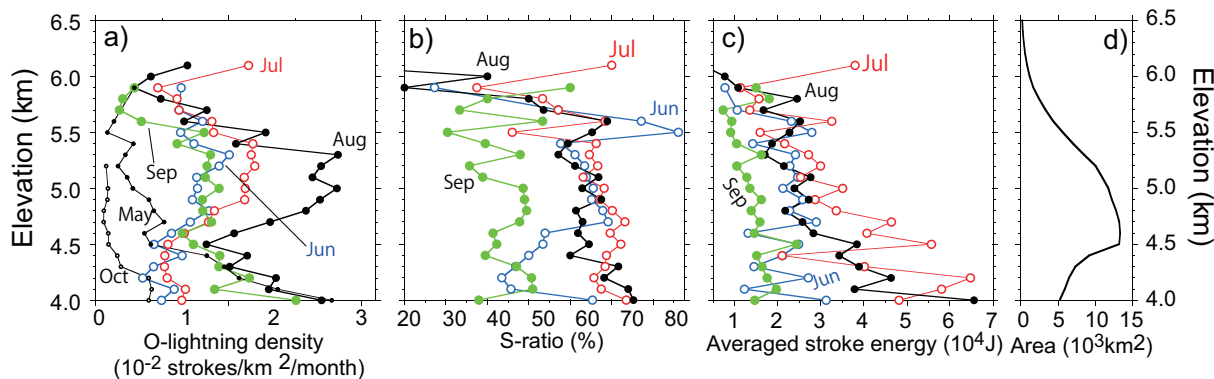


Fig. 10. Same as Fig. 8, but for HM region.

decrease significantly as the SSI and vertical wind shear increase (Figs. 13a, b, 14a, b). Since a large

SSI prohibits the initiation and development of deep convection, as is well known, these negative correla-

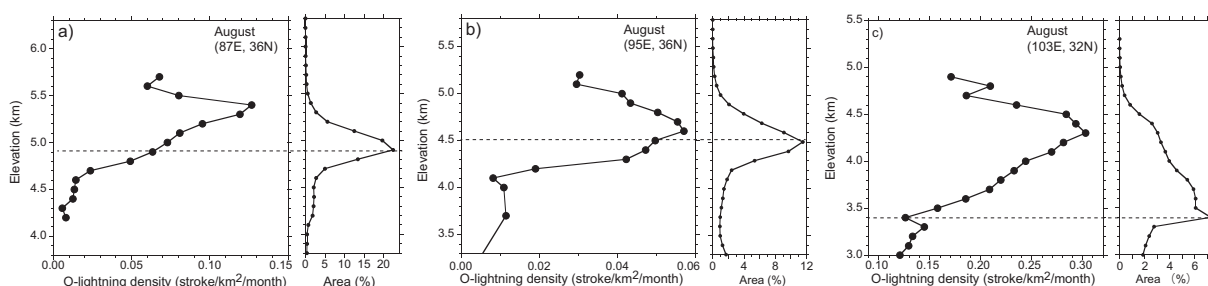


Fig. 11. Elevation profiles of O-lightning density in August (left panels) and area of each elevation zone (right panels) for three analysis units (A–C) in Fig. 1.

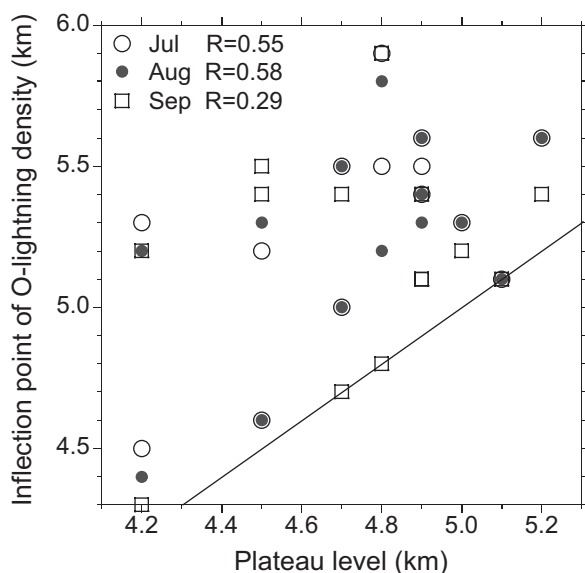


Fig. 12. Relation between plateau levels and maximum O-lightning density levels for 14 analysis units.

tions are to be expected. The vertical wind shear shows no significant correlation with the SSI ( $R < 0.017$ ) and directly influences the lightning activity. Large vertical wind shear is an important source of turbulent kinetic energy, which dilutes the in updraft air in convection during the initial stage of development. Since large vertical wind shear may also inhibit the initiation of deep convection, the negative correlations shown in Figs. 14a and 14b are to be expected.

The relations between the atmospheric conditions and lightning strengths show different behaviors. Both the S-ratio and average stroke energy exhibit negative correlations with vertical wind shear at 0.01 % significance (Figs. 14c, d) but are not correlated with SSI

(Figs. 13c, d).

## 5. Summary

The relation between lightning features and topography over the Tibetan Plateau was studied using the WLLN dataset obtained from April 2009 until December 2014. The analysis region was divided into three sub-regions: the HM, CT, and ET regions. The following observations were made:

1. The O-lightning density over the Tibetan Plateau was generally high ( $>10^{-1}$  stroke  $\text{km}^{-2} \text{yr}^{-1}$ ) except in the western part. Minimum density zones ( $<10^{-1.5}$  stroke  $\text{km}^{-2} \text{yr}^{-1}$ ) were observed along the Himalayas more than 6 km ASL and in deep valleys within the Tibetan Plateau. These areas corresponded to the areas of maximum and minimum GSMaP rainfall.
2. S-lightning over the Tibetan Plateau occurred more frequently ( $>10^{-1.5}$  stroke  $\text{km}^{-2} \text{yr}^{-1}$ ) than in the surrounding areas. The measured S-ratios in the analysis units generally exceeded 30 %; in particular, the S-ratio over the southern part of the Tibetan Plateau, including the Himalayas, was extremely high at 50 %.
3. For the areas less than 3 km ASL in all three sub-regions, O-lightning frequently occurred between 20 and 02 LST in JJA with relatively small S-ratios (below 20 %). In contrast, for the areas more than 4 km ASL, O-lightning frequently occurred between 14 LST and 20 LST in JJA, and the S-ratios exceeded 45 % from 15 LST to 18 LST.
4. The O-lightning density over the Tibetan Plateau reached a maximum at elevations about 0.2–1.0 km higher than the local plateau level in July and August.
5. The O-lightning and S-lightning densities were negatively correlated with the vertical wind shear

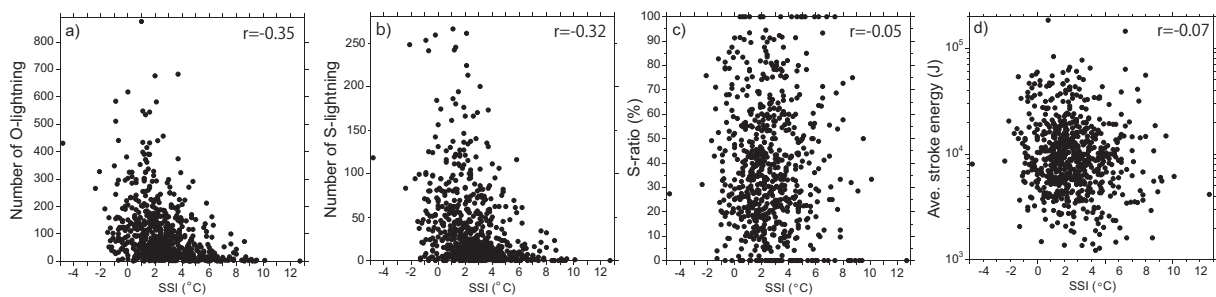


Fig. 13. Relation between SSI and lightning parameters around Nagqu sonde observation site at 18 LST (12 UTC) in JJAS. Lightning parameters are (a) number of O-lightning events, (b) number of S-lightning events, (c) S-ratio, and (d) average stroke energy. Number of data points is 694.

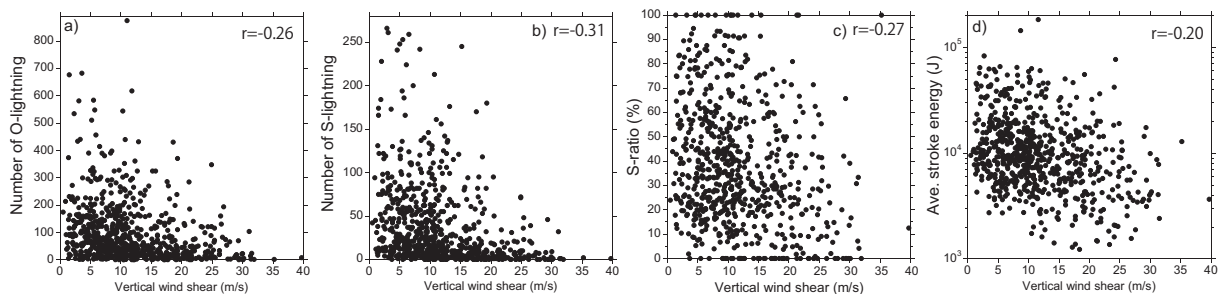


Fig. 14. Same as Fig. 13, but for vertical wind shear.

and the SSI around the Nagqu sonde site. However, the S-ratio was negatively correlated with the vertical wind shear only.

### Acknowledgments

This research was supported by a Grant-in-Aid for Scientific Research (C) 26400463. The author wishes to thank the World Wide Lightning Location Network (<http://wwlln.net>) — a collaboration of over 50 universities and institutions — for providing the lightning location data used in this study.

### References

- Abarca, S. F., K. L. Corbosiero, and T. J. Galarneau, Jr., 2010: An evaluation of the Worldwide Lightning Location Network (WWLLN) using the National Lightning Detection Network (NLDN) as ground truth. *J. Geophys. Res.*, **115**, D18206, doi:10.1029/2009JD013411.
- Aonashi, K., J. Awaka, M. Hirose, T. Kozu, T. Kubota, G. Liu, S. Shige, S. Kida, S. Seto, N. Takahashi, and Y. N. Takayabu, 2009: GSMaP passive microwave precipitation retrieval algorithm: Algorithm description and validation. *J. Meteor. Soc. Japan*, **87A**, 119–136.
- Becker, J. J., D. T. Sandwell, W. H. F. Smith, J. Braud, B. Binder, J. Depner, D. Fabre, J. Factor, S. Ingalls, S.-H. Kim, R. Ladner, K. Marks, S. Nelson, A. Pharaoh, R. Trimmer, J. von Rosenberg, G. Wallace, and P. Weatherall, 2009: Global bathymetry and elevation data at 30 arc seconds resolution: SRTM30\_PLUS. *Mar. Geod.*, **32**, 355–371.
- Bhatt, B. C., and K. Nakamura, 2005: Characteristics of monsoon rainfall around the Himalayas revealed by TRMM precipitation radar. *Mon. Wea. Rev.*, **133**, 149–165.
- Christian, H. J., R. J. Blakeslee, D. J. Boccippio, W. L. Boeck, D. E. Buechler, K. T. Driscoll, S. J. Goodman, J. M. Hall, W. J. Koshak, D. M. Mach, and M. F. Stewart, 2003: Global frequency and distribution of lightning as observed from space by the Optical Transient Detector. *J. Geophys. Res.*, **108**, 4005, doi:10.1029/2002JD002347.
- Dowden, R. L., J. B. Brundell, and C. J. Rodger, 2002: VLF lightning location by time of group arrival (TOGA) at multiple sites. *J. Atmos. Sol. Terr. Phys.*, **64**, 817–830.
- Hirose, M., and K. Nakamura, 2005: Spatial and diurnal

- variation of precipitation systems over Asia observed by the TRMM Precipitation Radar. *J. Geophys. Res.*, **110**, D05106, doi:10.1029/2004JD004815.
- Houze, R. A., D. C. Wilton, and B. F. Smull, 2007: Monsoon convection in the Himalayan region as seen by the TRMM Precipitation Radar. *Quart. J. Roy. Meteor. Soc.*, **133**, 1389–1411.
- Hutchins, M. L., R. H. Holzworth, C. J. Rodger, and J. B. Brundell, 2012a: Far field power of lightning strokes as measured by the World Wide Lightning Location Network. *J. Atmos. Oceanic Technol.*, **29**, 1102–1110.
- Hutchins, M. L., R. H. Holzworth, J. B. Brundell, and C. J. Rodger, 2012b: Relative detection efficiency of the World Wide Lightning Location Network. *Radio Sci.*, **47**, RS6005, doi:10.1029/2012RS005049.
- Iwasaki, H., 2014: Preliminary study on features of lightning discharge around Japan using World Wide Lightning Location Network data. *SOLA*, **10**, 98–102.
- Iwasaki, H., 2015: Climatology of global lightning classified by stroke energy using WWLLN data. *Int. J. Climatol.*, **35**, 4337–4347.
- Iwasaki, H., and T. Miki, 2002: Diurnal variation of convective activity and precipitable water over the “semi-basin” —Preliminary study on the mechanism responsible for the evening convective activity maximum—. *J. Meteor. Soc. Japan*, **80**, 439–450.
- Kubota, T., S. Shige, H. Hashizume, K. Aonashi, N. Takahashi, S. Seto, M. Hirose, Y. N. Takayabu, T. Ushio, K. Nakagawa, K. Iwanami, M. Kachi, and K. Okamoto, 2007: Global precipitation map using satelliteborne microwave radiometers by the GSMaP Project: Production and validation. *IEEE Trans. Geosci. Remote Sens.*, **45**, 2259–2275.
- Orville, R. E., and R. W. Henderson, 1986: Global distribution of midnight lightning: September 1977 to August 1978. *Mon. Wea. Rev.*, **114**, 2640–2653.
- Qie, X., R. Toumi, and T. Yuan, 2003: Lightning activities on the Tibetan Plateau as observed by the lightning imaging sensor. *J. Geophys. Res.*, **108**, 4551, doi:10.1029/2002JD003304.
- Rodger, C. J., J. B. Brundell, R. L. Dowden, and N. R. Thomson, 2004: Location accuracy of long distance VLF lightning location network. *Ann. Geophys.*, **22**, 747–758.
- Sato, T., and F. Kimura, 2005: Diurnal cycle of convective instability around the central mountains in Japan during the warm season. *J. Atmos. Sci.*, **62**, 1626–1636.
- Shrestha, M., K. Takara, T. Kubota, and S. Bajracharya, 2011: Verification of GSMaP rainfall estimates over the central Himalayas. *J. Japan Soc. Civ. Eng., Ser. B1*, **67**, I\_37–I\_42.
- Singh, P., and K. Nakamura, 2009: Diurnal variation in summer precipitation over the central Tibetan Plateau. *J. Geophys. Res.*, **114**, D20107, doi:10.1029/2009JD011788.
- Toumi, R., and X. Qie, 2004: Seasonal variation of lightning on the Tibetan Plateau: A Spring anomaly? *J. Geophys. Res.*, **31**, L04115, doi:10.1029/2003GL018930.
- Ushio, T., K. Sasashige, T. Kubota, S. Shige, K. Okamoto, K. Aonashi, T. Inoue, N. Takahashi, T. Iguchi, M. Kachi, R. Oki, T. Morimoto, and Z. Kawasaki, 2009: A Kalman filter approach to the Global Satellite Mapping of Precipitation (GSMaP) from combined passive microwave and infrared radiometric data. *J. Meteor. Soc. Japan*, **87A**, 137–151.
- Virts, K. S., J. M. Wallace, M. L. Hutchins, and R. H. Holzworth, 2013: Highlights of a new ground-based, hourly global lightning climatology. *Bull. Amer. Meteor. Soc.*, **94**, 1381–1391.
- Yamada, H., and H. Uyeda, 2006: Transition of the rainfall characteristics related to the moistening of the land surface over the central Tibetan Plateau during the summer of 1998. *Mon. Wea. Rev.*, **134**, 3230–3247.
- Yanai, M., and C. Li, 1994: Mechanism of heating and the boundary layer over the Tibetan Plateau. *Mon. Wea. Rev.*, **122**, 305–323.